The Journal of Physiology

Induced *in vivo* knockdown of the *Brca1* gene in skeletal muscle results in skeletal muscle weakness

Michael D. Tarpey[1], Ana P. Valencia[3], Kathryn C. Jackson[3], Adam J. Amorese[1], Nicholas P. Balestrieri[1], Randall H. Renegar[4], Stephen J. P. Pratt[5], Terence E. Ryan[1], Joseph M. McClung[1,2], Richard M. Lovering[5] and Espen E. Spangenburg[1,2]

[1] *Department of Physiology, Brody School of Medicine, East Carolina University, Greenville, NC, USA*
[2] *East Carolina Diabetes and Obesity Institute, Brody School of Medicine, East Carolina University, Greenville, NC, USA*
[3] *School of Public Health, Department of Kinesiology, University of Maryland, College Park, MD, USA*
[4] *Department of Anatomy and Cell Biology, Brody School of Medicine at East Carolina University, Greenville, NC, USA*
[5] *School of Medicine, Department of Orthopedics, University of Maryland, Baltimore, MD, USA*

Edited by: Michael Hogan & Russell Hepple

Key points

- Breast cancer 1 early onset gene codes for the DNA repair enzyme, breast cancer type 1 susceptibility protein (BRCA1). The gene is prone to mutations that cause a loss of protein function.
- BRCA1/Brca1 has recently been found to regulate several cellular pathways beyond DNA repair and is expressed in skeletal muscle.
- Skeletal muscle specific knockout of *Brca1* in mice caused a loss of muscle quality, identifiable by reductions in muscle force production and mitochondrial respiratory capacity.
- Loss of muscle quality was associated with a shift in muscle phenotype and an accumulation of mitochondrial DNA mutations.
- These results demonstrate that BRCA1 is necessary for skeletal muscle function and that increased mitochondrial DNA mutations may represent a potential underlying mechanism.

Abstract Recent evidence suggests that the breast cancer 1 early onset gene (*BRCA1*) influences numerous peripheral tissues, including skeletal muscle. The present study aimed to determine whether induced-loss of the breast cancer type 1 susceptibility protein (Brca1) alters skeletal muscle function. We induced genetic ablation of exon 11 in the *Brca1* gene specifically in the skeletal muscle of adult mice to generate skeletal muscle-specific *Brca1* homozygote knockout (Brca1KO^{smi}) mice. Brca1KO^{smi} exhibited kyphosis and decreased maximal isometric force in limb muscles compared to age-matched wild-type mice. Brca1KO^{smi} skeletal muscle shifted toward an oxidative muscle fibre type and, in parallel, increased myofibre size and reduced capillary numbers. Unexpectedly, myofibre bundle mitochondrial respiration was reduced,

Michael Tarpey completed his Master's degree in Exercise Physiology at the University of Hertfordshire, UK, before pursuing a PhD in Molecular and Cellular Science at Virginia Tech. Following the completion of his PhD in 2015, Michael took a postdoctoral position in the laboratory of Dr Espen Spangenburg at the East Carolina Diabetes and Obesity Institute (ECDOI), East Carolina University. Beyond investigating the role of BRCA1 in skeletal muscle, Michael's research is focused on understanding the mechanistic relationship between skeletal muscle function and mitochondrial bioenergetics.

DOI: 10.1113/JP276863

whereas contraction-induced lactate production was elevated in Brca1KO^{smi} muscle. Brca1KO^{smi} mice accumulated mitochondrial DNA mutations and exhibited an altered mitochondrial morphology characterized by distorted and enlarged mitochondria, and these were more susceptible to swelling. In summary, skeletal muscle-specific loss of Brca1 leads to a myopathy and mitochondriopathy characterized by reductions in skeletal muscle quality and a consequent kyphosis. Given the substantial impact of *BRCA1* mutations on cancer development risk in humans, a parallel loss of BRCA1 function in patient skeletal muscle cells would potentially result in implications for human health.

(Received 18 July 2018; accepted after revision 19 November 2018; first published online 22 November 2018)
Corresponding author Espen E. Spangenburg: East Carolina Diabetes and Obesity Institute, Department of Physiology, Brody School of Medicine, East Carolina University, Greenville, NC 27834, USA.
Email: spangenburge14@ecu.edu

Introduction

Breast cancer 1 early onset gene (*BRCA1*, *human*) codes for the large, multidomain breast cancer type 1 susceptibility protein (BRCA1) and is highly susceptible to genetic mutation in humans, with over 1600 mutations having been identified (Godet & Gilkes, 2017). Although some of these mutations are somatic (Hennessy *et al.* 2010; Bell *et al.* 2011), most *BRCA1* mutations are germ line (Satagopan *et al.* 2001) and result in a non-functional BRCA1 protein or complete loss of BRCA1 protein content as a result of protein instability (Yoshikawa *et al.* 1999; Godet & Gilkes, 2017). As a tumor suppressing protein, a central physiological function of BRCA1 is the repair of DNA (Wang *et al.* 2000; Liu & West, 2002; Kim *et al.* 2004; Yoshida & Miki, 2004; Saha *et al.* 2010; Roy *et al.* 2012); thus, the loss of BRCA1 function or protein content results in genomic instability and a greater risk of developing breast cancer and, to a lesser extent, ovarian cancer (Silver & Livingston, 2012). Historically, most studies have therefore focused on understanding the link between BRCA1 and cancer development in reproductive tissues. However, BRCA1 is expressed in all cell types and with varying levels of expression dependent on cell type (Anon, 2018). Recent studies have thus expanded the physiological role and necessity of BRCA1/Brca1 beyond DNA repair and reproductive tissues, describing a polyfunctional protein involved in the regulation of adipose, brain, smooth vascular muscle, cardiac muscle and skeletal muscle (Shukla *et al.* 2011; Ortega *et al.* 2012; Jackson *et al.* 2014; Lovren *et al.* 2014; Suberbielle *et al.* 2015).

BRCA1 is found on chromosome 17q21 and contains 24 exons, 22 of which code for the protein (Miki *et al.* 1994). Exon 11 is the largest and accounts for more than 60% of the 1863 amino acid polypeptide (Miki *et al.* 1994; Mehrgou & Akouchekian, 2016). At the nucleotide level, the murine form of Brca1 contains 72% sequence identity with the human form, with an amino acid similarity greater than 80% (Szabo *et al.* 1996). The RING domain of BRCA1 facilitates E3-ubquitin ligase activity (Freemont, 2000; Ruffner *et al.* 2001), whereas the tandem BRCT (C-terminus) domains allow for complex formation with phosphorylated proteins (Dulic *et al.* 2001; Manke *et al.* 2003; Yu *et al.* 2003; Williams *et al.* 2005). Together, these domains allow BRCA1 to regulate multiple distinct cellular functions (Venkitaraman, 2002; Deng, 2006). The regions of *BRCA1* coding for exons 11–13 and the RING and tandem BRCT domains are not only the most functionally relevant, but also the most frequently mutated (Clark *et al.* 2012). These features of *BRCA1*/BRCA1 necessitate further exploration to fully understand the scope and scale of BRCA1-regulated cellular processes in tissues throughout the body, as well as the potential consequences on systemic health in individuals with a loss of BRCA1 function or protein content.

As in the reproductive tissue, BRCA1 shares a pivotal role in DNA repair in non-reproductive tissues. For example, Brca1 supports neural integrity and cognitive function in mice via protection of the neural genome, which experiences frequent double-strand breaks (DSBs) following heightened neural activity (Suberbielle *et al.* 2015).

DSBs are similarly elevated in human atrial biopsies following ischaemic stress, and are associated with significantly increased BRCA1 expression (Shukla *et al.* 2011). Cardiomyocyte-specific Brca1 knockout (KO) mice suggest that this upregulation is necessary for Brca1-mediated DSB repair because loss of BRCA1 results in reduced DSB repair and impaired cardiac muscle remodelling, leading to increased mortality following cardiac ischaemia (Shukla *et al.* 2011). Brca1 has also been implicated in the protection of smooth muscle against oxidative stress (Lovren *et al.* 2014) and the attenuation of high-fat diet-induced aortic plaque lesions, as well as improved capillary density and blood flow following hind-limb ischaemia in mice (Singh *et al.* 2013). The range of cellular functions influenced by BRCA1/Brca1 also extends to metabolic pathways, regulating lipid metabolism in human breast cancer cells (MCF7)

(Magnard *et al.* 2002; Moreau *et al.* 2006) and lipid biosynthesis in adipose tissue via direct interactions between the BRCT domain and phosphorylated acetyl CoA carboxylase (p-ACC) (Ortega *et al.* 2012). Despite the growing significance of BRCA1 in the regulation of numerous cellular functions across multiple tissues, as well as the involvement of skeletal muscle in the progression and development of a host of diseases and co-morbidities, the literature concerning the role of BRCA1 within skeletal muscle remains sparse.

To date, our laboratory has shown that BRCA1 and Brca1 are expressed in human and murine skeletal muscle, respectively, and also that Brca1 localizes within skeletal muscle to the nucleus and mitochondria (Jackson *et al.* 2014, 2018). Furthermore, we have identified BRCA1/Brca1 as a regulator of skeletal muscle metabolism via BRCA1–p-ACC interactions (Jackson *et al.* 2014) and shown that skeletal muscle-specific loss of Brca1 protects mice against high-fat diet-induced perturbations in glucose and insulin tolerance (Jackson *et al.* 2018). The extent of BRCA1/Brca1 regulation on skeletal muscle function remains largely unknown. For example, the central function of skeletal muscle is locomotion, and loss of skeletal muscle strength and quality is associated with increased mortality (Metter *et al.* 2002), although the effect of Brca1 loss on skeletal muscle strength and quality has not been investigated. Additionally, although Brca1 is a known modulator of skeletal muscle metabolism and localizes to mitochondria, the relationship between Brca1 and mitochondrial function is not well understood. In the present study, we utilized an inducible skeletal muscle specific KO mouse model (Brca1KO^{smi}) coupled with an integrative experimental approach aiming to determine whether the loss of Brca1 expression is critical for skeletal muscle function in adult mice.

Methods

Ethical approval and animal experiments

The authors understand the ethical standards under which *The Journal of Physiology* operates and confirm that the animal procedures adhered to in the present study conform with these standards. All animal procedures and their usage were approved by the Institutional Review Committee at East Carolina University (Animal Usage Protocol #Q332a). Animal care complied with the Guide for the Care and Use of Laboratory Animals by the Institute of Laboratory Animal Resources, Commission on Life Sciences, National Research Council (https://grants.nih.gov/grants/olaw/guide-for-the-care-and-use-of-laboratory-animals.pdf). The present study utilized a total of 70 animals, 54 HSA-mER-Cre-mER (+)-*Brca1*(fl$^+$/fl$^+$) mice and 16 HSA-mER-Cre-mER(+) *Brca1*(fl$^+$/fl$^-$) mice. Mice were bred on a C57BL/6NJ background, and were a mix of male and female mice aged 30–34 weeks (weighing 30–50 g) at the time of death. Mice were housed under a 12:12 h light/dark cycle at 22°C with access to food and water available *ad libitum*. Animals were killed via isoflurane-induced anaesthesia, followed by cervical dislocation.

Animal generation and genotyping

We used the previously described HSA-Cre(+)-*Brca1*(fl/fl) mice (Jackson *et al.* 2018). All animals were genotyped based on the presence of HSA-Cre, and hetero- and homozygote *Brca1* flox expression using genomic DNA. Cre-mediated recombination was confirmed via PCR analysis of genomic DNA using a DNA isolation kit (Qiagen, Valencia, CA, USA). Briefly, a short bout of tamoxifen delivery via I.P. injections results in the deletion of exon 11 in the *Brca1* gene. We have previously demonstrated that this model results in the deletion of Brca1 protein content specifically in the skeletal muscle with no off-target effects (Jackson *et al.* 2018). We confirmed the deletion of exon 11 in the current cohort of animals at 30–34 weeks of age via PCR-amplified verification of DNA recombination (data not shown), as described previously (Jackson *et al.* 2018). Successful knockdown of Brca1 mRNA was also confirmed in the plantaris muscle for each group (data not shown).

Experimental approach

Ten- to 12-week-old HSA- mER-Cre-mER(+) *Brca1*(fl$^+$/fl$^+$) and HSA- mER-Cre-mER(+) *Brca1*(fl$^+$/fl$^-$) male and female mice were injected for 5 consecutive days with 2 mg day^{-1} tamoxifen or vehicle solution. Mice were allowed to age for an additional 20 weeks prior to experimentation. We chose 20 weeks because we have previously demonstrated that Brca1 protein was ablated from skeletal muscle 8 weeks post-tamoxifen treatment. Mice were placed under isoflurane-induced anaesthesia for the collection of muscle tissue, before being humanely killed. Animals of the genotype HSA- mER-Cre-mER(+) *Brca1*(fl$^+$/fl$^+$) administered tamoxifen or sunflower seed oil and ethanol are referred to as Brca1KO^{smi} and wild-type (WT) mice, respectively. Animals of genotype HSA- mER-Cre-mER(+) *Brca1*(fl$^+$/fl$^-$) administered tamoxifen are referred to as Het mice. Those mice administered vehicle are referred to as WT mice. In addition, a cohort of HSA- mER-Cre-mER(+) was assessed to ensure no off target effects of tamoxifen delivery. To date, we have found no effect of the tamoxifen delivery in any of our outcome measurements, including treadmill running, mitochondrial respiration, organ mass and/or body weight (data not shown).

Muscle fibre size and type

Muscle fibre cross-sectional area (CSA) and muscle fibre type were measured in the tibialis anterior (TA) muscle as a result of mixed muscle fibre type, as described previously (Schmidt *et al.* 2017). Images of muscle cross-sections were taken by a blinded investigator from six different locations across the belly of the muscle section and were probed with primary antibodies against myosin heavy chain type I (BA-F8), IIa (SC-71) and IIb (BF-F3) (Development Studies Hybridoma Bank, University of Iowa, Iowa City, IA, USA) and anti-dystrophin (Rb-9024; ThermoFisher, Waltham, MA, USA). Myosin heavy chain types I, IIa and IIb and dystrophin were stained with secondary fluorescence probes 350, 488, 546 and 647, respectively. Stained cross-sections were imaged using an EVOS FL automicroscope and the accompanying software (Life Technologies, Bothell, WA, USA). Fibre type and CSA were assessed using Image J (NIH, Bethesda, MD, USA), as described previously (Schmidt *et al.* 2017). All images were coded and randomized to allow for blinded analyses.

Histochemical staining of muscle fibres

TA tissue sections were stained with haematoxylin and eosin (H&E) in accordance with standard protocols. TA muscle collagen content was visualized using Sirius Red staining. Tissue sections stained for H&E and Sirius Red were imaged using standard light microscopy and analysed using ImageJ, version 1.6.0 (NIH). TA muscle was used for consistency across microscopy methods. The content of muscle fibres positive for the mitochondrial complexes cytochrome *c* oxidase (COX) and succinate dehydrogenase (SDH) was visualized using previously described methods (Otis *et al.* 2004). All images were coded and randomized to allow for blinded analyses.

Vascular density assessment

Vascular density was assessed in TA tissue by immunohistochemical staining, and is reported as the mean percentage $CD31^+$ (endothelial cell marker) per 20× field of view as described previously (Ryan *et al.* 2016). TA muscle was used for consistency across microscopy methods. All images were coded and randomized to allow for blinded analyses.

Isometric force production

Isometric force production was assessed *in vivo* for the plantar flexor muscles of WT and KO mice, as well as *in vitro* for extensor digitorum longus (EDL) muscles of WT, Het and KO mice, as described previously (Spangenburg *et al.* 2008; Iyer *et al.* 2016). For the *in vivo* experiments, mice were exposed to 4–5% isoflurane in an induction chamber and then placed on a nose cone for maintenance of anaesthesia using a precision isoflurane vaporizer. Toe pinch reflex was used to confirm proper anaesthetic depth. Optimal voltage was determined for each protocol. For the *in vivo* protocol, force was normalized to muscle mass as described previously as a result of the multiple muscle groups involved (Iyer *et al.* 2016).

In vitro fatigue resistance was assessed in EDL muscles for all three groups using a 10 min fatigue protocol consisting of 300 contractions at 30 Hz. Optimal voltage was determined for each protocol. Plantar flexor muscles were used for their capacity to measure isometric force *in vivo*. EDL muscles were used for *in vitro* measurements because it is easy to excise and tie are both proximal and distal tendons without damaging the muscle. For the *in vitro* protocol, muscle length and mass were recorded for the calculation of physiological CSA and specific force, expressed as N cm^{-2} (Barton *et al.* 2008).

Muscle lactate assay

Muscle lactate production was assessed by measuring the change in lactate present in the contractile bath media before and after the 10 min fatigue protocol in EDL muscles. Muscle lactate was measured using a Lactate Assay Kit (MAK064-1KT; Sigma-Aldrich, St Louis, MO, USA) in accordance with the manufacturer's instructions and normalized to the EDL muscle mass.

Preparation of permeabilized muscle fibre bundles

Permeabilized muscle fibre bundles were prepared from portions of the medial gastrocnemius muscle as a result of its oxidative phenotype and ease of mechanical fibre separation, as described previously (O'Rourke *et al.* 2018). Medial gastrocnemius muscle was used because of its predominantly red phenotype. Medial gastrocnemius muscle was excised and placed in ice-cold buffer X [in mM: 7.23 K_2EGTA, 2.77 CaK_2EGTA, 20 imidazole, 20 taurine, 5.7 ATP, 14.3 phosphocreatine, 6.56 $MgCl_2{\cdot}6H_2O$ and 50 Mes, pH 7.1, 295 mosmol $(kgH_2O)^{-1}$]. Connective tissue and fat were removed using a dissecting microscope, and fibre bundles of ∼1 mg wet weight were separated using microdissecting tweezers. Muscle fibre bundles were permeabilized in buffer X containing 30 $\mu g\ mL^{-1}$ saponin with continuous rotation at 4°C for 30 min. Muscle bundles were promptly transferred to ice-cold buffer Z [in mM: 110 K-Mes, 35 KCl, 1 EGTA, $5K_2HPO_4$, 3 $MgCl_2{\cdot}6H_2O$ and 5 mg mL^{-1} BSA, pH 7.4, 295 mosmol $(kgH_2O)^{-1}$] and washed with continuous rotation at 4°C for 15 min.

High-resolution respirometry

High-resolution respirometry measurements were made on permeabilized muscle fibre bundles using the

OROBOROS Oxygraph-2K (Oroboros Instruments, Innsbruck, Austria) as described previously (O'Rourke *et al.* 2018). Experiments were conducted at 37°C with a starting oxygen concentration of ∼300–350 μM in buffer Z, containing 20 mM creatine monohydrate and 25 μM blebbistatin. Mitochondrial respiration was assessed by the sequential addition of substrates at a final concentration of 4 mM pyruvate, 0.5 mM malate, 5 mM glutamate, 2.5 mM ADP, 5 mM succinate, 5 μM cytochrome *c*, 10 μM rotenone, 5 μM anti-mycin A, 2 mM ascorbic acid and 0.5 mM TMPD (*N*,*N*,*N*′,*N*′-tetramethyl-*p*-phenylenediamine dihydrochloride). Mitochondrial membrane integrity was confirmed by the addition of exogenous cytochrome *c*. Muscle fibre bundles that produced a >10% increase in respiration were excluded. Muscle fibre bundles were rinsed in distilled H_2O, freeze-dried (Labconco, Kansas City, MO, USA) and weighed (Orion Cahn C-35; Thermo Electron, Beverly, MA, USA). O_2 consumption rates were normalized to dry weight and converted to pmol s^{-1} mg^{-1} dry weight O_2. All chemicals and reagents were purchased from Sigma-Aldrich.

Mitochondrial H_2O_2 production

Mitochondrial H_2O_2 emission was measured fluorometrically in permeabilized muscle fibre bundles, as described previously (O'Rourke *et al.* 2018). Briefly, muscle fibre bundles were placed in 1 mL cuvettes containing Amplex Ultra Red (25 μM), horseradish peroxidase (1 U mL^{-1}) and blebbistatin (25 μM) at 37°C, and mixed using a magnetic stirrer. Resorufin fluorescence was detected at Ex:EM 565:600 via a spectrofluorometer (SPEX Fluoromax 3; HORIBA Jobin Yvon, Kyoto, Japan). Mitochondrial H_2O_2 emission was stimulated through the addition of succinate (10 mM) and mitochondrial H_2O_2 buffering capacity was assessed via the addition of thioredoxin reductase and glutathione reductase inhibitors, auranofin (AF) (1 μM) and carmustine (BCNU) (100 μM), respectively. Fibre bundles were rinsed in distilled H_2O, freeze-dried and weighed after each experiment. Standard curves were generated and fluorescence was converted to nM mg^{-1} dry weight H_2O_2. Scavenger index, a measure of H_2O_2 buffering capacity, was calculated as the percentage change in resorufin fluorescence between succinate and the succinate + AF/BCNU stages.

Skeletal muscle mitochondrial isolation

Skeletal muscle mitochondria were isolated as described previously (Hepple *et al.* 2015). Freshly isolated mitochondria were used for the osmotic swelling assay and the remaining isolate was stored at –80°C for assessment of mitochondrial DNA (mtDNA) mutations.

Mitochondrial osmotic swelling assay

Mitochondrial osmotic swelling was measured using a protocol adapted from one described previously (Lee *et al.* 2005). Briefly, 250 μg of isolated mitochondria was incubated in 1 mL of KCl buffer (in mM: 140 KCl and 3 Hepes, pH 7.4) at room temperature and mixed via a magnetic stir bar. Following a brief background measure, $CaCl_2$ was added (final concentration of 200 μM), after which 3.125 μg of alamethicin was added following a further measuring period. Mitochondrial swelling as a result of solute flux in and out of the mitochondrial matrix was recorded by the change in absorbance at $\lambda_{540\ nm}$ using a spectrofluorometer. Rates of swelling were calculated based on the Δabsorbance$_{540\ nm}$ min^{-1} between the initial linear background rate and the rate following the addition of $CaCl_2$. ΔAbsorbance$_{540\ nm}$ was normalized to maximal mitochondrial swelling, as determined via the addition of alamethicin.

Mitochondrial DNA mutations assay

The mutation frequency in mtDNA was measured using an adaptation of a protocol described previously (Vermulst *et al.* 2008). Isolated mitochondria were processed using a Qiagen minispin kit (model 27104) in accordance with the manufacturer's recommendations for the extraction of mtDNA. Mutations were detected via a quantitative PCR assay using primer sets mControl forward: TCGGCGTAAAACGTGTCAAC; mControl reverse: CCGCCAAGTCCTTTGAGTTT; mTaq634 forward: ACTCAAAGGACTTGGCGGTA; and mTag634 reverse: AGCCCATTTCTTCCCATTTC. Mitochondrial DNA isolated from 1-year-old C57BL/6 and old Polg mutator mice served as negative and positive controls, respectively. Polg mutator mice are known to accumulate significant mtDNA mutations by 1 year of age as a result of the expression of a proofreading-deficient version of polymerase gamma (Trifunovic *et al.* 2004; Kujoth *et al.* 2005)

Electron microscopy

Soleus muscle was used because of its high mitochondrial content. The soleus was cut into 1–2 mm strips and fixed for 1–3 hours at 4°C in a solution of 2% glutaraldehyde in 0.1 M sodium cacodylate buffer (pH 7.4). After rinsing, tissues were post-fixed in a solution of 1% osmium tetroxide (Stevens Metallurgical, New Yor, NY, USA) in 0.1 M sodium phosphate buffer (pH 7.4). Rinsed tissues were then dehydrated by passage through a graded ethanol series and embedded in Spurr's media (Electron Microscopy Sciences, Hatfield, PA, USA). Ultra-thin sections (70 nm) were placed on 200-mesh copper grids coated with Coat Quick 'G' (Daido Sangyo Co., Kawasaki, Japan)

Table 1. Immunohistochemical antibodies source information

Antibody	Vendor	Catalogue number and reference code	Dilution factor
Myosin heavy chain type I	Development Studies Hybridoma Bank, University of Iowa (Iowa City, IA, USA)	#BA-F8 RRID:AB_10572253	1:50
Myosin heavy chain type IIa		#SC-71 RRID:AB_2147165	1:50
Myosin heavy chain type IIb		#BF-F3 RRID:AB_2266724	1:50
Anti-dystrophin	ThermoFisher (Waltham, MA, USA)	#Rb-9024-P RRID:AB_149805	1:50
Alexa Fluor 350	ThermoFisher	#A-21140 RRID:AB_2535777	1:250
Alexa Fluor 488	ThermoFisher	#A-21121 RRID:AB_2535764	1:250
Alexa Fluor 546	ThermoFisher	#A-21045 RRID:AB_2535714	1:250
Alexa Fluor 647	ThermoFisher	#A-21245 RRID:AB_141775	1:250

and then stained sequentially by immersion in 2% aqueous uranyl-acetate followed by Reynold's lead citrate. Grids were examined in a Jeol 1200 EX electron microscope (Jeol Inc., Peabody, MA, USA) at an accelerating voltage of 80 kV, and images were recorded using a MegaView III CCD camera (Olympus, Tokyo, Japan) and iTEM software (Soft Imaging Systems, Münster, Germany).

Muscle homogenization and western blotting

TA muscles were excised and immediately flash frozen. Samples were stored at –80°C. Muscle samples were placed in ice-cold cell lysis buffer (50 mM Tris-HCl, EDTA 1 mM, NaCl 150 mM, SDS 0.1%, sodium deoxycholate 0.5%, igepel Ca 630 1%, pH 7.5) containing protease and phosphatase inhibitors. Samples were homogenized and centrifuged. Protein concentrations were determined via a bicinchoninic acid assay (ThermoFisher). Proteins (20–30 μg) were separated on SDS-PAGE gels (Criterion TGX Stain-Free Gels; Bio-Rad, Hercules, CA, USA), which were photo-activated prior to transfer to polyvinylidene difluoride (PVDF) membranes (Trans-Blot Turbo Transfer System; Bio-Rad). PVDF membranes were imaged to record total lane protein before being blocked at room temperature for 1 h in 5% non-fat dry milk or 5% BSA, and then incubated overnight with primary antibodies (Table 1) at 4°C. Following primary antibody incubation, membranes were incubated at room temperature for 1 h with goat anti-rabbit HRP-conjugated secondary antibodies (ab97051; Abcam, Cambridge, MA, USA) at concentrations of 1:2000 to 1:20,000. Proteins were visualized via chemiluminescence with care being taken to ensure signal detection was in a linear range and not saturated (Clarity Western ECL Substrate, Bio-Rad; SuperSignal West Femto, ThermoFisher). Captured ECL signals were quantified using Image Lab Software, version 5.2.1 (Bio-Rad) and normalized to total lane protein content. See Table 2 for primary antibodies used, dilation factors and exposure times.

Statistical analysis

D'Agostino–Pearson omnibus tests were conducted to confirm that data followed a normal distribution. Student's *t* tests were used to analyse differences between WT and KO groups when data were normally distributed. One-way analysis of variance tests were used to analyse differences in contractile function and mitochondrial respiration between the WT, Het and KO groups when data were normally distributed. Multiple comparisons were made using Sidak *post hoc* tests. Data that did not follow a normal distribution were analysed using a Mann–Whitney *U* test when comparing WT and KO groups only, and a Kruskal–Wallis test with Dunn's multiple comparisons when comparing WT, Het and KO groups. Statistical analyses were conducted using Prism, version 7.03 (GraphPad Software Inc., San Diego, CA, USA). The α level was set at 0.05. All data are reported as the mean ± SEM.

Results

Brca1KO^{smi} mice develop kyphosis and altered skeletal muscle size

Twenty weeks post-tamoxifen injection, Brca1KO^{smi} mice developed kyphosis, which was not seen in WT mice

Table 2. Western blot primary and secondary antibodies source information

Antibody	Vendor	Catalogue number and reference code	Dilution factor and exposure time
4-HNE (4-hydroxynonenal)	Abcam (Cambridge, MA, USA)	#Ab46545 RRID:AB_722490	1:3000 75 s
APE1 (apurinic/apyrimidinic endonuclease)	Abcam	#Ab137708 RRID:AB_2732912	1:1000 5 s
TTC11/Fis1 (mitochondrial fission 1 protein)	Abcam	#Ab71498 RRID: AB_1271360	1:1000 30 s
Glutathione reductase	Abcam	#Ab137513 RRID:AB_2732913	1:1000 20 s
NTH1 (endonuclease III-like protein 1)	Abcam	#Ab191413 RRID:AB_2732911	1:1000 5 s
Ogg1 (8-oxoguanine glycosylase)	Abcam	#Ab135940 RRID:AB_2732910	1 ug/ml 15 s
Parkin	Abcam	#Ab15954 RRID:AB_443270	1:1000 15 s
p-Parkin Ser^{65}	Abcam	#Ab154995 RRID:AB_2732915	1:1000 6 s
TXNRD1 (thioredoxin reductase 1)	Abcam	#Ab124954 RRID:AB_10975643	1:1000 5 s
TXNRD2 (thioredoxine reductase 2)	Abcam	#Ab180493 RRID:AB_2732914	1:1000 10 s
Goat anti-rabbit HRP-conjugated secondary antibody	Abcam	#ab97051 RRID:AB_10679369	1:2000 – 1:20,000
Drp1 (dynamin-related protein 1)	Cell Signaling (Beverly, MA, USA)	#8570s RRID:AB_10950498	1:500 60 s
p-Drp1 Ser^{616}	Cell Signaling	#3455 RRID:AB_2085352	1:1000 6 s
MFN2 (mitofusin-2)	Cell Signaling	#9482s RRID:AB_2747394	1:1000 30 s
OPA1 (optic atrophy type 1)	Cell Signaling	#80471 RRID:AB_2734117	1:1000 10 s

20 weeks post-vehicle injection (Fig. 1*A*), nor was it identified in Cre(+) animals injected with tamoxifen (data not shown). The development of kyphosis occurs for a variety of reasons, although commonly as a result of muscle weakness. Thus, we aimed to determine whether loss of Brca1 altered the overall phenotype of the skeletal muscle. The absolute mass of the gastrocnemius, quadriceps and TA muscles was similar between WT and Brca1KO^{smi} groups (Fig. 1*B* and *C*). However, both overall TA muscle diameter and TA muscle fibre CSA were significantly greater in Brca1KO^{smi} compared to WT skeletal muscle (Fig. 1*D* and *E*). In agreement, Brca1KO^{smi} skeletal muscle exhibited a rightward shift in the frequency distribution of individual muscle fibre size compared to the WT mice (Fig. 1*F* and *G*). Because the muscle in the Brca1KO^{smi} exhibited significant increases in muscle fibre size without changes in muscle mass, we assessed differences in collagen content in each group. We found no quantitative differences in the total amount of Sirius Red staining between groups, suggesting no differences in collagen content (Fig. 1*H* and *I*).

Brca1KO^{smi} mice display an altered skeletal muscle fibre phenotype

Next, we assessed whether there were differences in skeletal muscle fibre type between WT and Brca1KO^{smi} mice in TA muscle. The skeletal muscle of Brca1KO^{smi} had significantly fewer type IIb fibres relative to WT skeletal muscle with no significant differences in the other fibre type populations (Fig. 2*A* and *B*). In addition, COX and SDH staining showed a pattern of expression, also supporting a shift in muscle fibre type. Skeletal muscle from Brca1KO^{smi} possessed significantly fewer negative COX and SDH fibres, at the same time as also possessing a significantly greater percentage of strong staining COX and SDH fibres (++) (Fig. 2*C* and *D*). Because capillary density often follows muscle fibre type, we assessed the number of capillaries (CD31+ cells) in the muscle cross-sections. We found a trend toward reduced capillaries content in TA muscle cross-sections ($P = 0.07$); however, when corrected to the fibre number, we found a significantly reduced capillary

density in Brca1KO^{smi} compared to WT skeletal muscle (Fig. 2*E*–*G*).

Isometric force production is reduced and fatigue resistance is increased in Brca1KO^{smi} skeletal muscle

To assess whether the altered Brca1KO^{smi} phenotype impacted muscle force production, we measured isometric force of the plantar flexor group and EDL muscle using an *in situ* stimulation platform and an *in vitro* approach, respectively. Normalized muscle force was significantly lower in Brca1KO^{smi} compared to WT mice using both the *in vivo* (g/muscle) and *in vitro* (N/cm^2) approaches (Fig. 3*A* and *B*). Reductions in specific force were not significant between WT and Het EDL muscle. Fatigue resistance, measured in the same pool of EDL muscles, demonstrated significantly greater fatigue resistance in EDL muscles of the Brca1KO^{smi} mice (Fig. 3*C*), whereas no differences were observed between WT and Het mice.

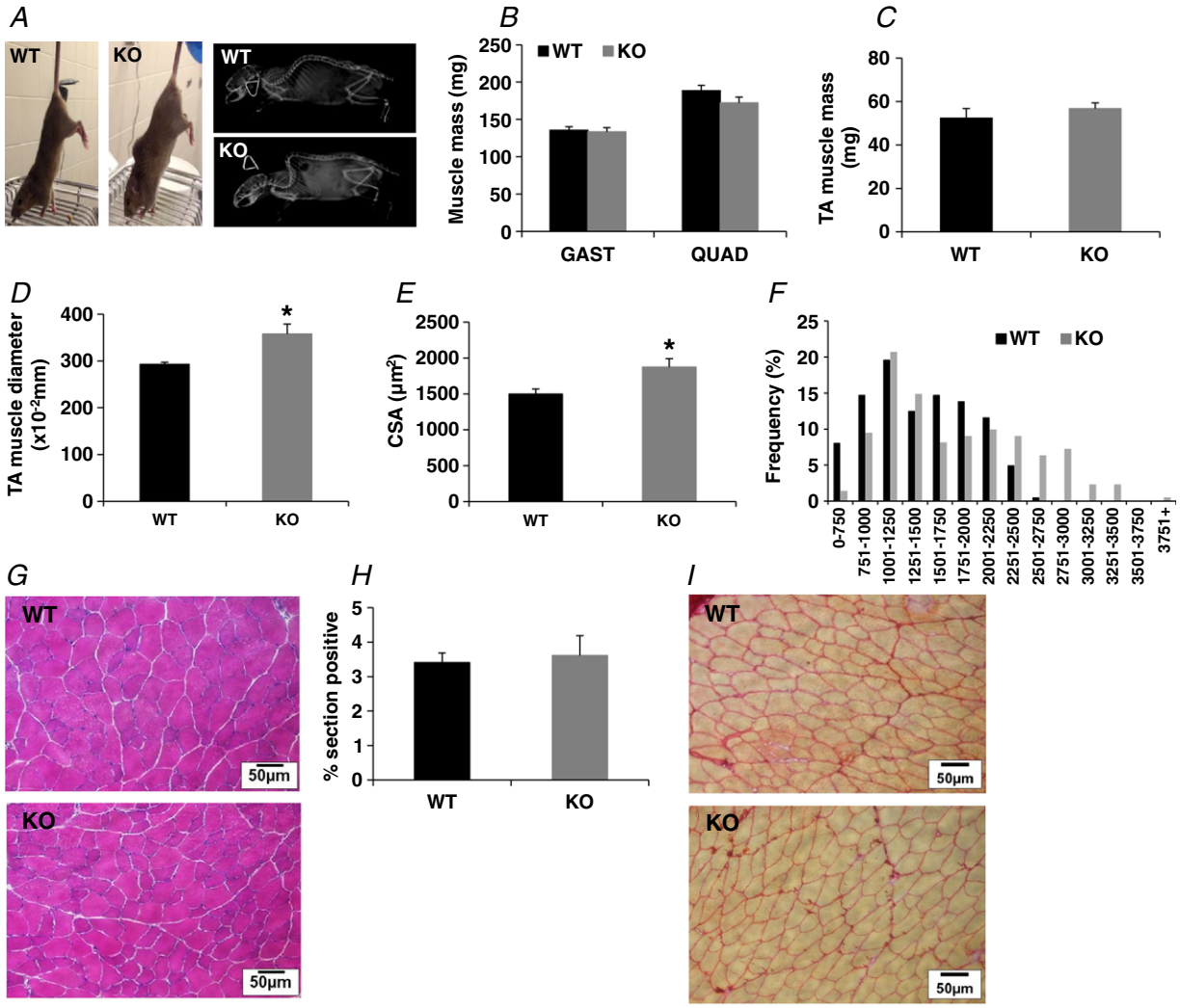

Figure 1. Brca1KO^{smi} develop kyphosis and altered skeletal muscle characteristics compared to aged-matched WT mice

Representative photographs and X-ray images show the development of kyphosis in Brca1KO^{smi} mice (*A*). Muscle mass of gastrocnemius ($n = 8$ per group), quadriceps ($n = 8$ per group) and TA ($n = 5$ per group) muscles was similar between WT and Brca1KO^{smi} mice (*B* and *C*). Despite a similar muscle mass, we found a significantly greater muscle diameter and muscle fibre CSA in TA muscles of Brca1KO^{smi} compared to WT mice (*D*–*F*). Representative images of H&E stained TA muscle cross-sections used for muscle CSA measurements are included (*G*). Collagen content was similar between WT and Brca1KO^{smi} mice (*H*). Representative images of TA muscle cross-sections ($n = 5$ per group) stained for collagen (*I*). Black bars refer to WT mice and grey bars refer to Brca1KO^{smi} mice. All images were coded and randomized to allow for blinded analyses. ∗Statistically different from WT ($P < 0.05$). Data are the mean ± SEM.

Lactate produced during the isometric contraction fatigue protocol (Fig. 3*D*) was increased in the EDL of Brca1KO^{smi} mice, suggesting that Brca1KO^{smi} may be more reliant on glycolytic metabolism compared to WT mice.

Brca1KO^{smi} mice exhibit a unique mitochondrial phenotype showing reduced respiratory function

Our previous data in human primary myotubes (Jackson *et al.* 2014) and isolated mitochondria (Jackson *et al.*

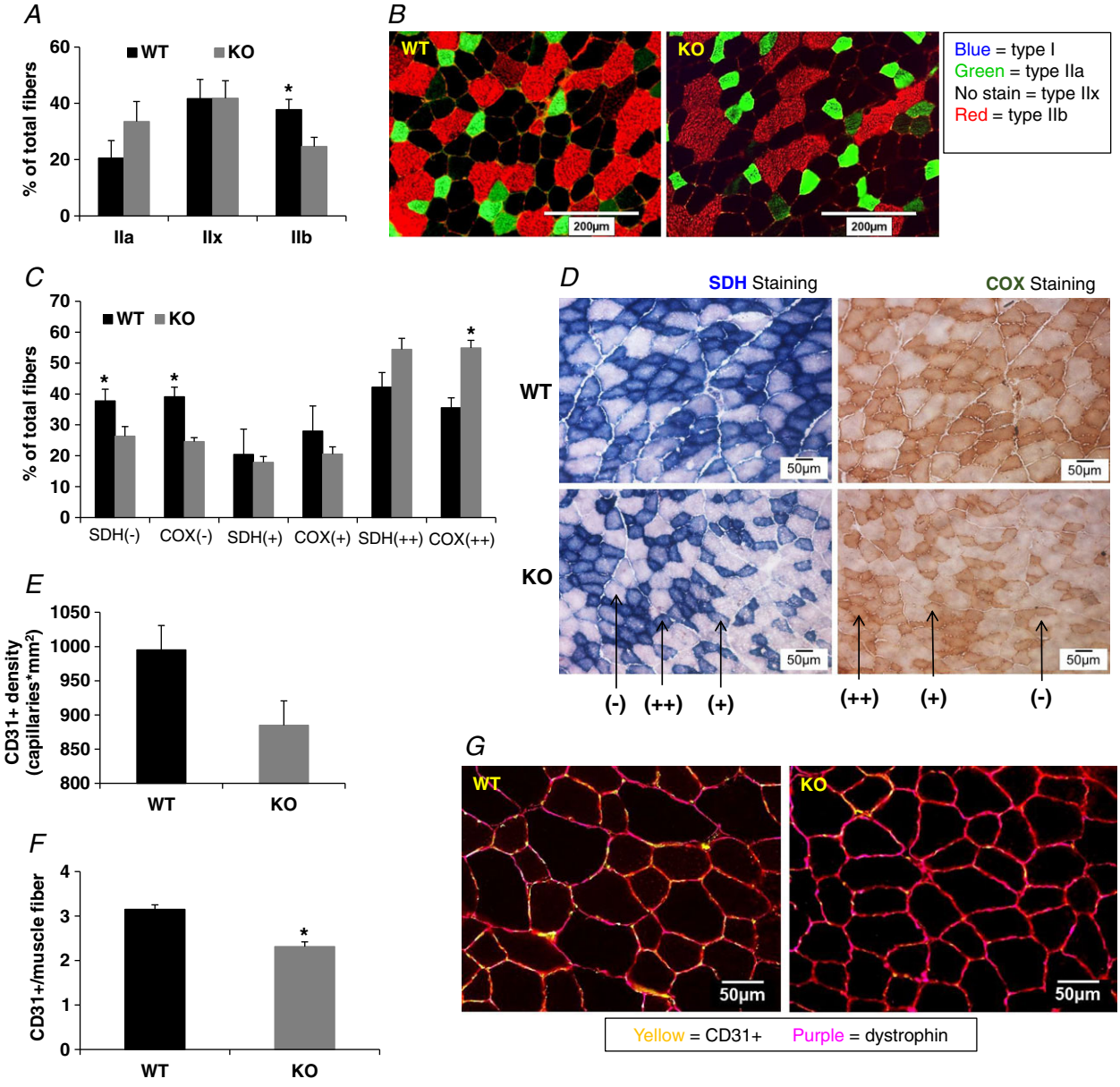

Figure 2. Brca1KO^{smi} mice display an altered skeletal muscle fibre phenotype compared to aged matched WT mice

Myosin heavy chain (MHC) labelling of TA muscle cross-sections shows significant muscle fibre type shifts in Brca1KO^{smi} mice (*A*). Representative immunofluorescence MHC images (*B*) are labelled as: blue = type I, green = type IIa, no stain = IIx and red = IIb. SDH and COX staining of WT and Brca1KOsmi muscle cross-sections supports a shift toward an oxidative phenotype in Brca1KO^{smi} skeletal muscle (*C*). Representative images of SDH and COX staining (*D*) are labelled as: blue = SDH and brown = COX. Capillary number per mm^2, based on CD31$^+$ positive staining, trended lower in Brca1KO^{smi} muscle (*E*) and was significantly lower when CD31$^+$ was corrected to muscle fibre number (*F*). Representative images (purple/red = dystrophin and green/yellow = CD31$^+$) demonstrate the significant reductions in capillary density following Brca1 ablation (*G*). Black bars refer to WT mice and grey bars refer to Brca1KO^{smi} mice. All images were coded and randomized to allow for blinded analyses. *Statistically different from WT ($P < 0.05$). Data are the mean ± SEM.

2018) suggest that oxidative capacity might be uniquely affected in the Brca1KO^{smi} mice; thus, we aimed to directly assess mitochondrial respiration. Accordingly, we employed a permeabilized muscle fibre bundle approach to assess mitochondrial respiration (because it maintains the mitochondria in their native state at the same time as still maintaining the natural architecture of the muscle cell). Using fibre bundles prepared from the medial portion of the gastrocnemius muscle, we found that O_2 consumption from muscle fibre bundles of Brca1KO^{smi} mice was lower compared to the WT and Het animals (Fig. 4*A–E*). Specifically, mitochondrial respiration was significantly lower during state 3 respiration at complexes I compared to WT mice, and complexes I+II, II and IV relative to WT and Het mice. Respiration was comparable between WT and Het mice. We also assessed mitochondrial H_2O_2 emission potential and found no significant differences between the WT, HET or KO mice following the addition of either succinate (Fig. 4*F*) or thioredoxin reductase and glutathione reductase inhibitors, AF and BCNU, respectively (Fig. 4*G*). However, scavenger index, a representation of H_2O_2 buffering capacity, was significantly elevated in KO mice compared to WT and Het mice (Fig. 4*H*).

Brca1KO^{smi} mitochondria show abnormal morphology, a greater accumulation of mtDNA mutations and increased Ca^{2+}-induced swelling

Using electron microscopy of soleus muscle, we observed that Brca1KO^{smi} muscle was characterized by morphologically abnormal mitochondria, displaying a fused and swollen reticulum compared to that of WT and Het animals. We observed similar mitochondrial morphology between WT and Het skeletal muscle, which was consistent with mitochondrial respiratory data (Fig. 5*A*). Because BRCA1/Brca1 is largely recognized as a DNA repair protein (Wang *et al.* 2000; Liu & West, 2002; Kim *et al.* 2004; Yoshida & Miki, 2004; Saha *et al.* 2010; Roy *et al.* 2012) and co-localizes with mitochondria and probably mtDNA (Coene *et al.* 2005; Maniccia *et al.* 2009; Jackson *et al.* 2018), we measured the frequency of mtDNA mutations in skeletal muscle. mtDNA was derived

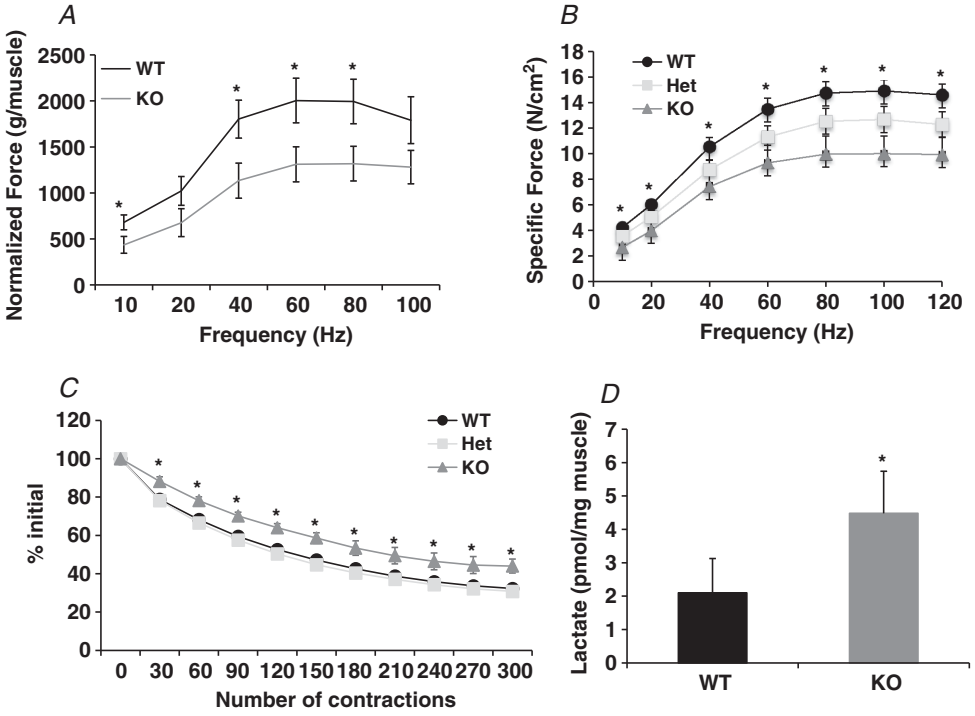

Figure 3. Altered contractile responses and lactate production in Brca1KO^{smi} skeletal muscle compared to skeletal muscle from aged matched WT mice
In vivo gastrocnemius/plantaris specific force production was significantly reduced in Brca1KO^{smi} ($n = 5$) compared to WT ($n = 4$) mice (*A*). *In vitro* isometric force production was similarly reduced in Brca1KO^{smi} ($n = 9$) EDL muscles (*B*); however, Het ($n = 11$) and WT ($n = 13$) muscles were not different. *In vitro* EDL fatigue resistance was significantly greater Brca1KO^{smi} mice compared to age-matched Het and WT mice (*C*). Significantly increased lactate production within Brca1KO^{smi} EDL muscles during the *in vitro* fatigue protocol suggests a greater reliance on glycolytic metabolism (*D*). Black bars refer to WT mice, light grey bars refer to Het and dark grey bars refer to Brca1KO^{smi} mice. *Statistically different from WT ($P < 0.05$). Data are the mean ± SEM.

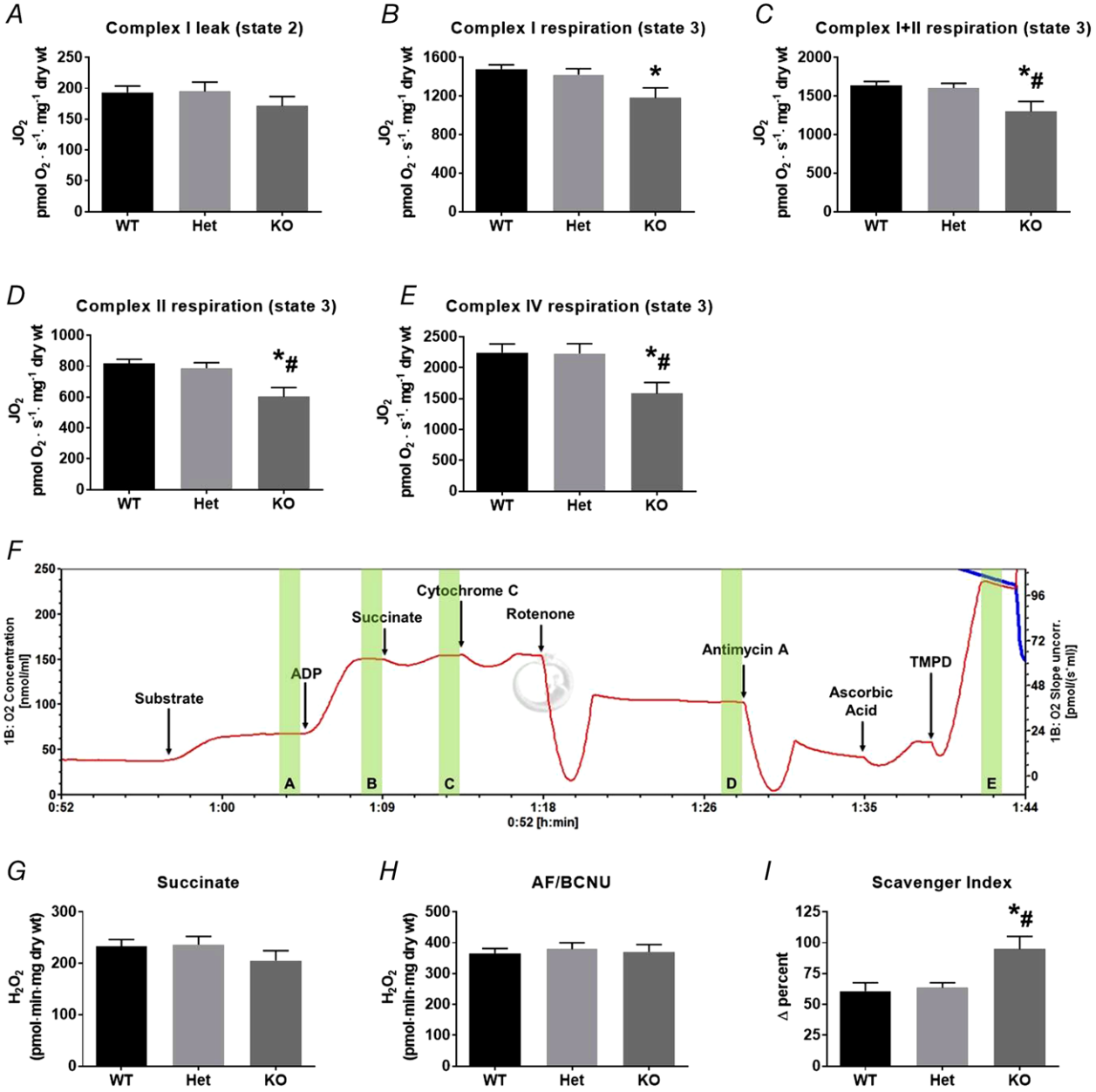

Figure 4. Skeletal muscle mitochondrial respiration and H_2O_2 emission in Brca1KO^{smi} mice
Medical gastrocnemius muscle fibre bundles from WT (n = 15), Het (n = 16) and KO (n = 14) mice were separated and permeabilized in preparation for high-resolution respirometry and H_2O_2 emission. Substrates and inhibitors were added sequentially to measure complex I leak and ADP-stimulated complexes I, I+II, II and IV mitochondrial respiration, as well as H_2O_2 emission. Data were corrected to muscle dry weight. Complex I leak (state 2) respiration was similar between WT, HET and Brca1KO^{smi} fibre bundles (*A*); however, complex I (state 3) respiration (*B*), complex I+II (state 3) respiration (*C*), complex II (state 3) respiration (*D*) and complex IV (state 3) respiration (*E*) were significantly lower in Brca1KO^{smi} fibre bundles. Representative tracing of high-resolution respirometry measurement with regions of interest labelled (*A*) to (*E*) to identify the corresponding image (*F*). H_2O_2 emission was not different between groups under succinate-only (*G*) or succinate + AF/BCNU (thioredoxin and glutathione reductase inhibitors, respectively) *H*, scavenger index, calculated as the percentage difference in H_2O_2 emission following the addition of AF/BCNU inhibitors, was significantly increased in BCRA1KO^{smi} compared to Het and WT fibre bundles (*I*). Black bars refer to WT mice, light grey bars refer to Het and grey bars refer to Brca1KO^{smi} mice. *Statistically different from Het ($P < 0.05$). Data are the mean ± SEM. [Colour figure can be viewed at wileyonlinelibrary.com]

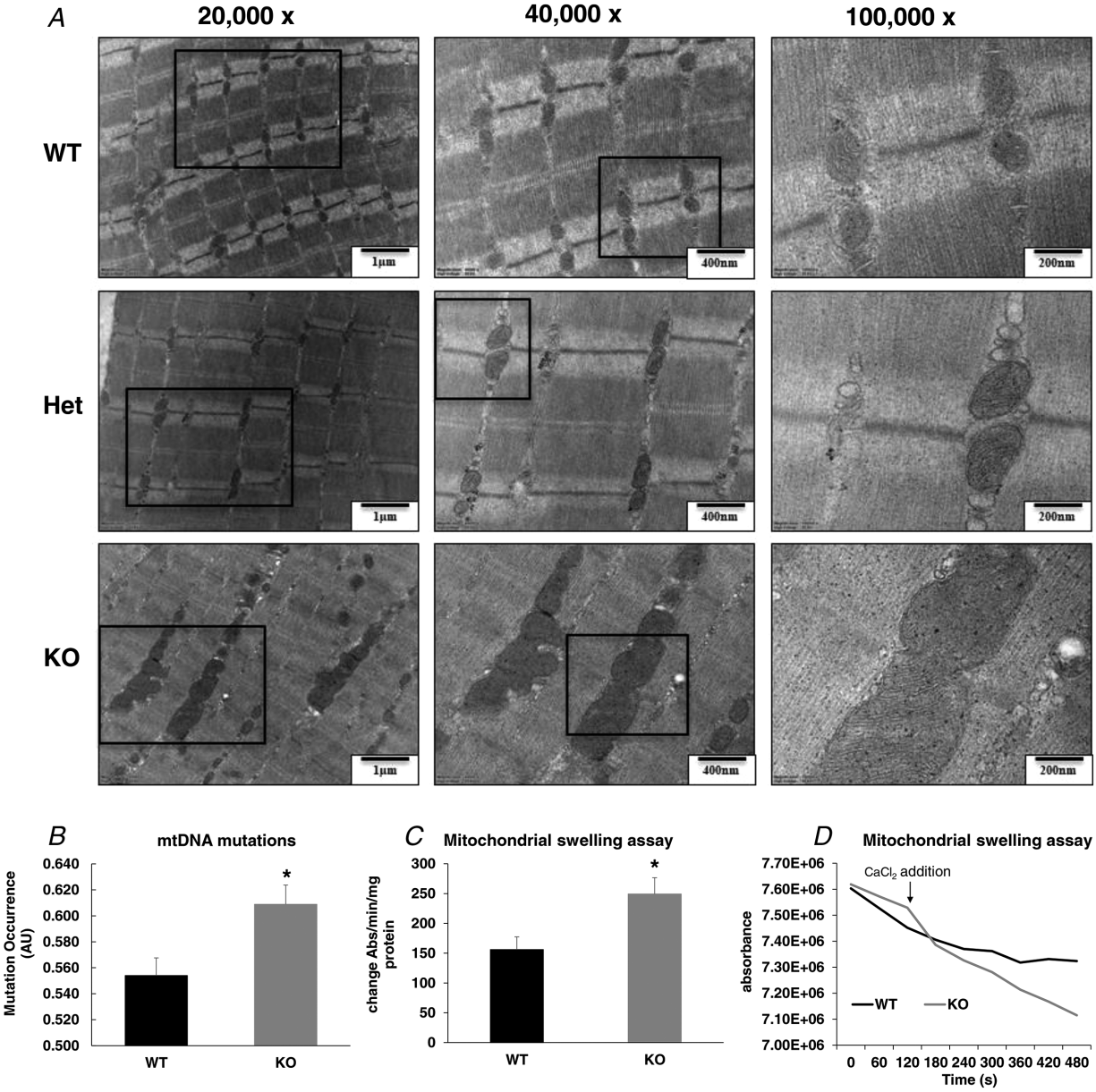

Figure 5. Mitochondrial morphology, DNA mutations and Ca^{2+}-induced swelling
Sections of soleus muscle were cut and fixed for imaging of mitochondrial morphology via transmission electron microscopy (TEM). Mitochondria were isolated from the skeletal muscle of age-matched WT ($n = 14$) and Brca1KO^{smi} ($n = 11$) mice for the assessment of mtDNAmutations. Isolated mitochondria were equilibrated in a KCl buffer before the addition of $CaCl_2$. Changes to solute flux in and out of the mitochondrial matrix were recorded by the change in absorbance at $\lambda_{540\ nm}$. $\Delta Absorbance_{540\ nm}$ was normalized to maximal mitochondrial swelling, determined via the addition of alamethicin. Lower absorbance equates to greater mitochondrion volume. Distinctive morphological shifts in the mitochondrial network were demonstrated via TEM images of soleus muscle cross-sections; images are presented for WT, Het and Brca1KO^{smi} mice at magnifications of 20,000×, 40,000× and 100,000×. Black boxes indicate magnified regions (*A*). Morphological shifts were associated with significant increases in mitochondrial DNA mutations in Brca1KO^{smi} mice (*B*). Mitochondria isolated from Brca1KO^{smi} muscle further showed an increased susceptibility to Ca^{2+}-induced swelling (*C* and *D*). Black bars refer to WT mice and grey bars refer to Brca1KO^{smi} mice. *Statistically different from WT ($P < 0.05$). Data are the mean ± SEM.

from isolated mitochondria sourced from red, white and mixed skeletal muscle from the hind- and forelimbs. Skeletal muscle from mBrca1KO^{smi} mtDNA contained a significantly greater mutational burden compared to the WT (Fig. 5*B*). Isolated mitochondria were suspended in KCl buffer and absorbance at λ_{540nm} was monitored to determine changes in mitochondrial volume via solute flux before and after the addition of Ca^{2+} ($CaCl_2$). Mitochondria isolated from Brca1KO^{smi} skeletal muscle were significantly more susceptible to Ca^{2+}-induced increases in mitochondrial volume (Fig. 5*C* and *D*).

Protein markers of DNA repair, anti-oxidant defence and oxidative stress are similar between Brca1KO^{smi} and WT mice

BRCA1 has previously been shown to have regulatory functions in pathways of genomic stability, including base excision repair (BER) (Saha *et al.* 2010), anti-oxidant defence (Bae *et al.* 2004; Gorrini *et al.* 2013) and cellular ROS levels (Saha *et al.* 2009). To further investigate the accumulation of mtDNA mutations in Brca1KO^{smi} mice, we measured key protein markers within these pathways from TA muscle homogenate (Fig. 6*A*). We examined the skeletal muscle protein content of the BER enzymes Ogg1, NTH1 and APE1. Ogg1, NTH1 and APE1 were all similar between Brca1KO^{smi} and WT mice (Fig. 6*B*–*D*). Protein levels of glutathione reductase (Fig. 6*E*), cytoplasmic thioredoxin reductase (Fig. 6*F*) and mitochondrial-localized thioredoxin reductase (Fig. 6*G*) were similar between Brca1KO^{smi} and WT mice. Finally, as a biomarker of oxidative stress, we measured the lipid peroxidation by-product, 4-HNE, which was similar between Brca1KO^{smi} and WT mice (Fig. 6*H*).

Protein markers of mitochondrial dynamics and mitophagy are altered in Brca1KO^{smi} skeletal muscle

In light of the alteration in mitochondrial morphology, we examined mitochondrial dynamics and mitophagy regulatory proteins by western blotting using TA muscle homogenate (Fig. 7*A*). OPA1, an inner mitochondrial membrane fusion protein, showed a strong trend toward greater protein content in Brca1KO^{smi} muscle ($P = 0.052$) (Fig. 7*B*). The outer mitochondrial membrane fusion regulator, MFN2, was similar between Brca1KO^{smi} and WT muscles (Fig. 7*C*). Drp1, a mitochondrial fission protein, and its phosphorylated form (Drp1^{S616}) were both significantly reduced in Brca1KO^{smi} muscles (Fig. 7*D* and *E*). Additionally, the mitochondrial fission protein, Fis1, which promotes Drp1 recruitment to the outer mitochondrial membrane (Palmer *et al.* 2013), was significantly reduced ($P = 0.016$) in muscle of Brca1KO^{smi} mice (Fig. 7*F*). Muscle protein content of the pro-mitophagy protein, Parkin, was not different between Brca1KO^{smi} and WT muscles. The phosphorylated form, Parkin^{S65}, was significantly elevated in Brca1KO^{smi} skeletal muscle (Fig. 7*G* and *H*).

Discussion

Using our recently described Brca1KO^{smi} mouse model (Jackson *et al.* 2018), we demonstrate that the loss of skeletal muscle BRCA1 protein leads to kyphosis associated with a decrease in force-producing capacity. This functional myopathy was accompanied by significant alterations in the overall phenotype of the skeletal muscle. Specifically, there was transition towards a more oxidative fibre type profile that was not accompanied by an increase in capillary density of the muscle. We discovered a consistent reduction across all of the muscle mitochondrial respiratory states assessed, suggesting the development of a mitochondriopathy. We found that Brca1KO^{smi} muscle mitochondria were visually swollen, contained a higher burden of mtDNA mutations and possessed a mitochondrial membrane more susceptible to osmotic swelling (as indicated by greater Ca^{2+}-induced membrane permeability). Together, our data demonstrate that KO of the *Brca1* gene leads to a skeletal muscle phenotype characterized by weaker muscles, reduced capillary density, and dysfunctional mitochondria with reduced oxidative capacities and mutated mitochondrial DNA.

Mutations in *BRCA1* have traditionally been considered in the context of breast and ovarian cancer development. With the exception of our previous studies (Jackson *et al.* 2014, 2018), little is known about Brca1 in skeletal muscle. The loss of skeletal muscle quality (i.e. force produced per mass of muscle) following the induced loss of Brca1 provides critical proof that Brca1 is critical for the maintenance of skeletal muscle function. The deterioration of muscle quality in the musculature of Brca1KO^{smi} mice probbaly led to the development of kyphosis. Indeed, muscle from Brca1KO^{smi} mice produced less force across most stimulation frequencies, regardless of whether muscle force was measured with direct or indirect electrical stimulation. It is noteworthy that the reduction in muscle force was largely the result of an increase in CSA, which produced a significantly lower specific force. The reduction in muscle force therefore is not a result of muscle atrophy but, instead, a loss of muscle quality. In a pre-clinical setting, these data provide a strong rationale for assessment of skeletal muscle function in individuals carrying *BRCA1* mutations that influence protein function. Het mice demonstrated a lower mean specific force compared to WT mice, and these differences were not significantly lower or higher than WT and Brca1KO^{smi} mice, respectively.

Brca1KO^{smi} developed an oxidative muscle fibre type profile characterized by greater COX/SDH staining and a reduction in IIb muscle fibres. However, greater muscle fibre CSA and reduced capillary density also developed, which is inconsistent with a more oxidative muscle phenotype (Schiaffino & Reggiani, 2011). The noted reduction in capillary density may have been an indirect result of Brca1 ablation because of a possible loss of cross-talk between endothelial and skeletal muscle cells. Unexpectedly, Brca1KO^{smi} muscle demonstrated greater fatigue resistance, which is expected with the oxidative fibre type, although this is at odds with the reduced capillary density. An increase in fatigue resistance is somewhat reconciled by the elevated lactate emitted by Brca1KO^{smi} muscle during fatiguing contractions, implying a greater reliance on glycolytic metabolism. Similar metabolic shifts have previously been reported following the ablation of BRCA1 in human smooth muscle cells (Lovren *et al.* 2014) and Brca1KO^{smi} mice (Jackson *et al.* 2018), whereas the overexpression of BRCA1 in cultured breast cancer cells downregulated glycolytic gene expression and upregulated oxidative gene expression (Privat *et al.* 2014). Increased lactate production/glycolytic metabolism following Brca1 loss may represent an adaptation to compromised mitochondrial function in Brca1KO^{smi} mice.

Impaired mitochondrial respiratory capacity is a further factor potentially contributing to the overall

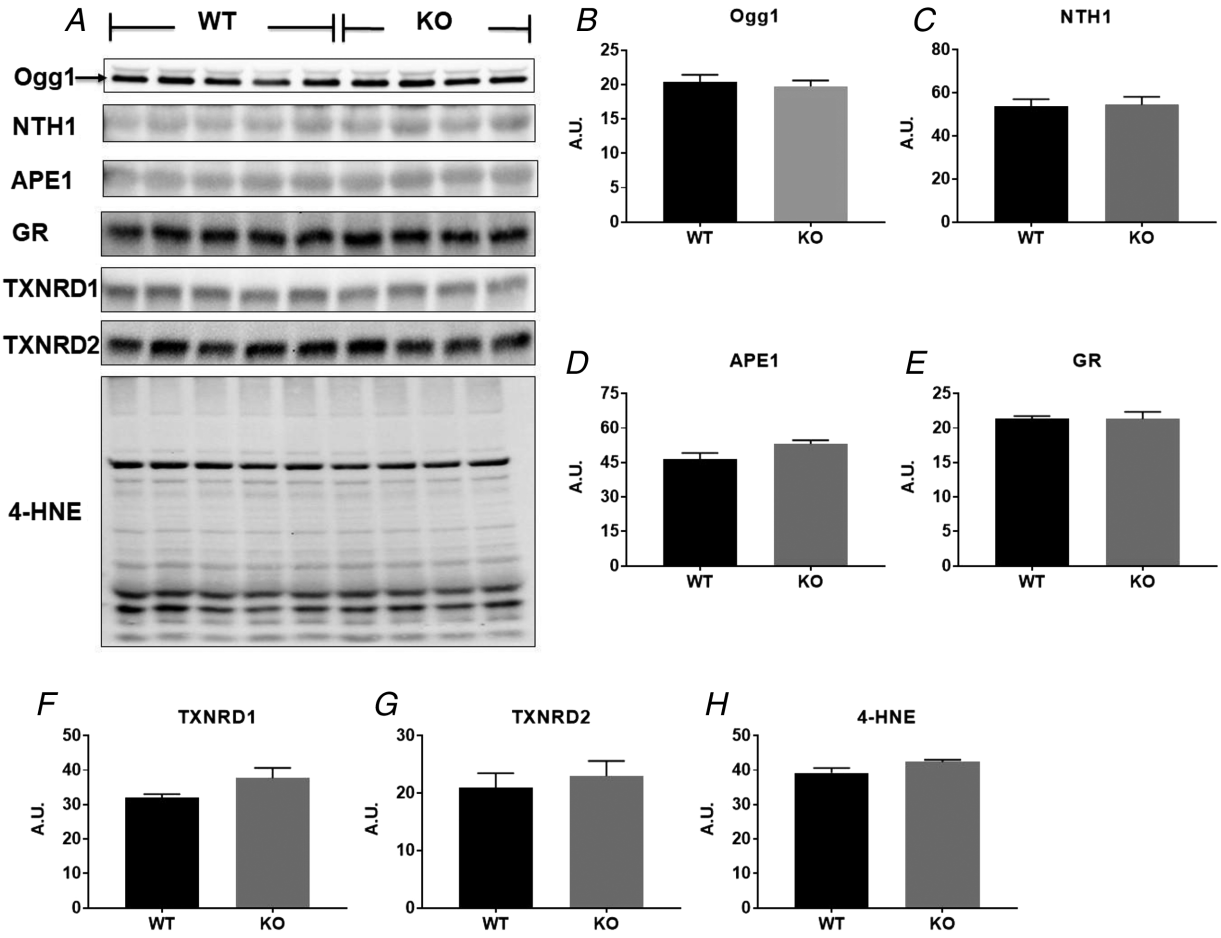

Figure 6. Protein markers of HER, anti-oxidant defence and oxidative stress
Whole muscle homogenate from TAmuscles of age-matched WT ($n = 5$) and Brca1Ko^{smi} ($n = 4$) mice was assessed for protein content of the BER enzymes, Oggl, NTH1 and APE1, anti-oxidant defence enzymes, glutathione reductase (GR), TXNRDI and TXNRD2, and a biomarker of oxidative stress, 4-HNE (*A*). The glycosylase, Oggl, was similar between WT and Brca1Ko^{smi} mice (*B*), in contrast to the glycosylase, NTH1 (*C*) and the endonuclease, APE1 (*D*), which were unchanged followed *Brca1* KO. Protein content of the anti-oxidant enzymes, glutathione reductase (GR), cytoplasm localized thioredoxin reductase (TXNRD1 and mitochondria localized thioredoxin reductase (TXNRD2) was similar between WT and Brca1KO^{smi} mice (*E–G*). The lipid peroxidationmarker, 4-HNE, was comparable between WT and Brca1KO^{smi} muscle, which may indicate similar states of oxidative stress (*H*). Black bars refer to WT mice and grey bars refer to Brca1KO^{smi} mice. *Statistically different from WT ($P < 0.05$). Data are the mean ± SEM.

loss of muscle quality in Brca1KO^{smi} mice. Using intact permeabilized muscle fibre bundles, we demonstrated respiratory impairments at complexes I, I+II, II and IV in Brca1KO^{smi} mice, supporting previous BRCA1/Brca1-loss studies in human myotubes (Jackson *et al.* 2014) and isolated mitochondria from Brca1KO^{smi} mice (Jackson *et al.* 2018). However, these data substantially extend previous results by assessing respiration using an approach that ensures the native reticular structure of the mitochondria is maintained without disrupting the architecture of the muscle fibre. In addition, the present study is the first to compare respiration rates in WT and Brca1KO^{smi} mice with those of heterozygote Brca1 mice. The comparable respiration rates between WT and Het mice indicate that Brca1 is not haploinsufficient in skeletal muscle. The difference in respiratory capacity between the WT and Brca1KO^{smi} is associated with a lower muscle quality. Similar findings have been reported in other animal models where mitochondrial respiration is compromised and associated with reduced specific force capacity that is not a result of muscle atrophy (Gouspillou *et al.* 2018). However, it should be noted that other models demonstrate muscle atrophy accompanied by reduced absolute force with reduced respiration kinetics, although a frequent key characteristic of these models is increased mortality (Diaz *et al.* 2005; Morrow *et al.* 2017). Mitochondrial respiratory dysfunction reported in Brca1KO^{smi} mice was associated with increased

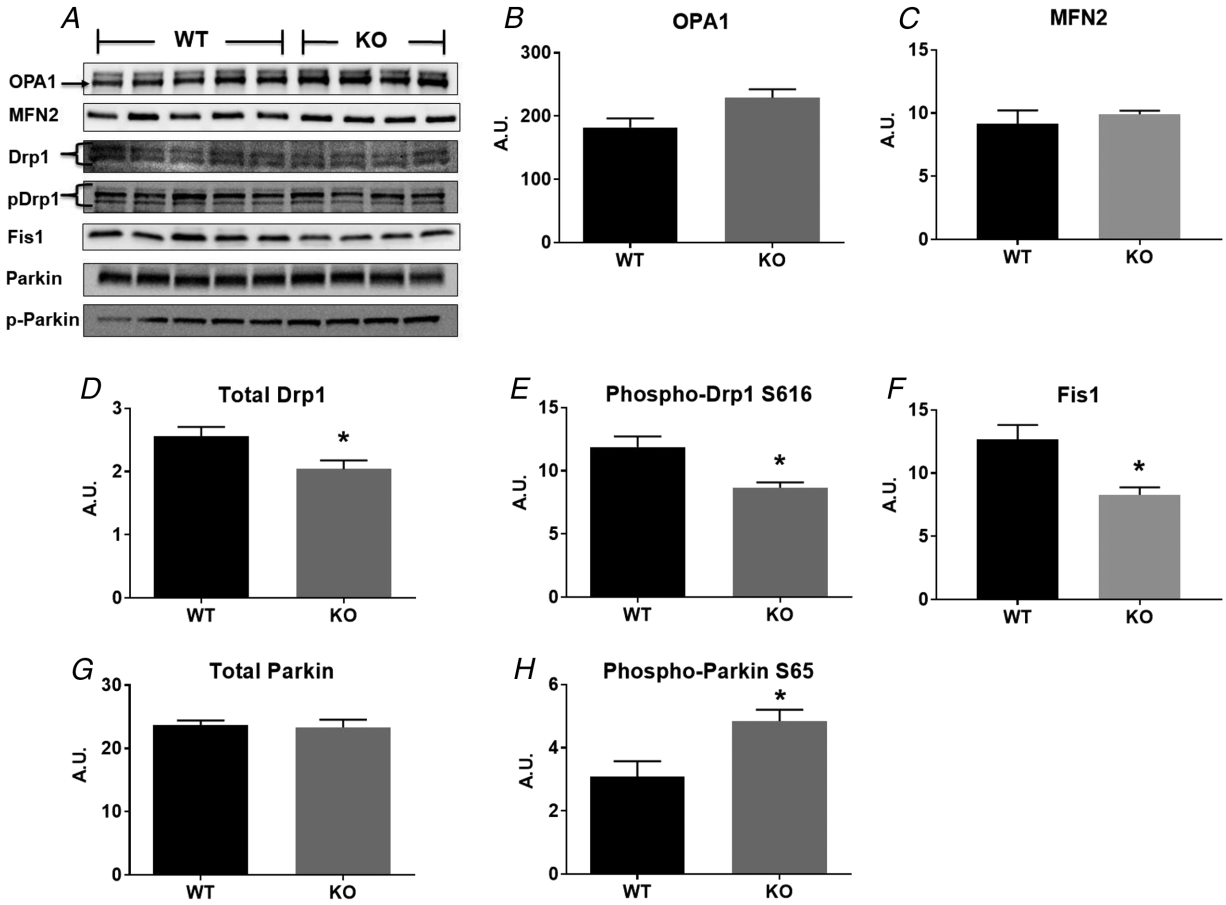

Figure 7. Mitochondrialdynamic and mitophagy protein markers in Brca1KO^{smi} skeletal muscle
Tibialis anterior muscles from age-matched WT ($n = 5$) and Brca1KO^{smi} ($n = 4$) mice were assessed via western blotting for specific protein markers of mitochondrial fusion (OPAl and MFN2), mitochondrial fission (Drp1 and Fis) and mitophagy (Parkin) (*A*). OPAl, an inner mitochondrial membrane fusion protein, showed a strong trend toward greater content in Brca1KO^{smi} muscle (*B*). MFN2, a regulator of outer mitochondrial membrane fusion, was similar between groups (*C*). The mitochondrial fission protein, Drp1, and its covalently active form, Drp1^{S616}, were both significantly lower in Brca1KO^{smi} muscle (*D* and *E*). Fis1, a mitochondrial fission promotor and Drp1 recruitment protein, was significantly lower in Brca1KO^{smi} muscle (*F*). The respective shifts in fusion and fission proteins imply a profusion state. Total protein content of the mitophagy marker, Parkin, was similar between groups (*G*), although a significant elevation in phospho-Parkin^{S65} (*H*) suggests that there may be greater initiation of mitophagy in Brca1KO^{smi} skeletal muscle. Black bars refer to WT mice and grey bars refer to Brca 1KO^{smi} mice. *Statistically different from WT ($P < 0.05$). Data are the mean ± SEM.

mtDNA mutations, altered mitochondrial morphology and increased Ca^{2+}-induced membrane permeability.

Mitochondrial DNA is particularly susceptible to oxidative damage (Saha *et al.* 2010; Alexeyev *et al.* 2013), partly because of its proximity to the major site of cellular ROS generation: the mitochondrion (Shokolenko *et al.* 2009). Using a permeabilized muscle fibre approach, we found no direct evidence of increased mitochondrial ROS emission in Brca1KO^{smi} skeletal muscle, although we did note a significant increase in the scavenger index, indicating greater superoxide quenching potential in Brca1KO^{smi} mice. Increased mtDNA mutations are probably not the result of increased ROS but, instead, may be a result of reduced repair. BER is the most prevalent mtDNA repair pathway (Alexeyev *et al.* 2013) and is a target of BRCA1 regulation. BRCA1 has previously been reported to stimulate the expression and activity of the BER enzymes, OGG1, NTH1 and APE1 in MCF-7 cells, whereas knockdown of *BRCA1* reduced enzyme expression (Saha *et al.* 2010). These data appear to contradict those obtained for Brca1KO^{smi} mice, which show similar OGG1, NTH1 and APE1 protein levels. Protein levels do not necessarily reflect enzyme activity and thus impaired BER cannot be ruled out as a mechanism of mtDNA mutation in Brca1KO^{smi} mice. Additionally, contradictions between past and current data may be the result of model and tissue-specific differences.

BRCA1 has also been reported to positively regulate anti-oxidant pathways via interactions with Nrf2 (Gorrini *et al.* 2013). Protein content for glutathione and thioredoxin reductases, which are transcription targets of Nrf2 (Ma, 2013), were unchanged between Brca1KO^{smi} and WT mice, implying that loss of BRCA1-Nrf2 anti-oxidant regulation may not be a key factor in the accumulation mtDNA mutations. These data are consistent with our H_2O_2 data in permeabilized muscle fibre bundles, which would have been expected to elicit increased H_2O_2 emission and reduced scavenger index relative to WT animals. Likewise, 4-HNE content between Brca1KO^{smi} and WT mice suggests that mtDNA mutations were not the result of oxidative stress from increased non-mitochondrial ROS or deficiencies in anti-oxidant defence pathways.

Analysis of mitochondrial dynamics proteins demonstrates altered regulation of the mitochondrial reticulum, which, in addition to greater membrane permeability, supports the enlarged/swollen morphological adaptations found in Brca1KO^{smi} skeletal muscle mitochondria. OPA1 and MFN2 are important regulators of inner mitochondrial membrane fusion (Neuspiel *et al.* 2005; Ishihara *et al.* 2006; Liu *et al.* 2009), whereas phosphorylation of Drp1 at serine 616 activates Drp1 fission activity (Taguchi *et al.* 2007; Kashatus *et al.* 2015), which is aided by Fis1-mediated Drp1 recruitment (Palmer *et al.* 2013). Respective shifts in the skeletal muscle content of these proteins support the fused appearance of the mitochondrial reticulum. The inferred increase in the activity of the mitophagy regulator, Parkin, as a result of increased S65 phosphorylation also suggests that Brca1KO^{smi} mitochondria may be in a pro-mitophagy state. Similarly, the knockdown of BRCA1 in fibroblasts increased the expression of autophagy markers, LC3 and LAMP1, and the mitophagy marker, BNIP3 (Salem *et al.* 2012), whereas LC3II was expressed following the knockdown of BRCA1 in breast cancer cells (Arun *et al.* 2015). Mitophagy induction is anticipated in response to mtDNA mutations (de Vries *et al.* 2012); however, mtDNA mutations continued to accumulate in Brca1KO^{smi} mice, which may be a result of incomplete autophagy/mitophagy activation (de Vries *et al.* 2012) or could reflect the severity of Brca1 ablation on mtDNA quality.

The Brca1KO^{smi} model used in the present study is specific to skeletal muscle, although muscle groups are not homogenous and, instead, vary considerably in key characteristics, such as fibre type, contractile strength and oxidative capacity. Adaptations to Brca1 ablation cannot therefore be assumed to occur equally across all muscle groups. Some conclusions, however, do presume a degree of extrapolation to provide potential mechanistic insights. This represents a limitation of the present study. Adaptations in Brca1KO^{smi} mice were found in TA, plantar flexor, EDL, gastrocnemius and soleus muscles. Furthermore, the development of kyphosis indicated that deleterious effects were not limited to the hind limbs. Together, these results suggest that shifts in muscle phenotype following the deletion of Brca1 are not confined to any particular muscle group, and thus it is expected that some uniformity in adaptations occurs across the muscles examined, although a very detailed analysis is necessary to confirm this idea.

In summary, skeletal muscle-specific ablation of Brca1 leads to a deterioration in skeletal muscle quality, which manifests physiologically as kyphosis and a reduction in isometric force output. Mitochondrial respiratory capacity is also reduced in Brca1KO^{smi} skeletal muscle, which is associated with an accumulation of mtDNA mutations and abnormal mitochondrial morphology. Muscle force production, mitochondrial respiration and H_2O_2 emission data, as well as mitochondrial morphology, were similar between WT and Het mice. These data suggest that, in skeletal muscle, Brca1 may not be haploinsufficient, as has previously been reported in MCF-7 and human breast epithelial cells (Cousineau & Belmaaza, 2007; Konishi *et al.* 2011), thereby implying that BRCA1/Brca1 haploinsufficiency may be cell or tissue-specific. Loss of BRCA1/Brca1 has previously been implicated in cognitive, cardiac and vascular health (Shukla *et al.* 2011; Singh *et al.* 2013; Suberbielle *et al.* 2015), as well as comprising a modulator of substrate metabolism and metabolic phenotype in adipose tissue

and skeletal muscle (Ortega *et al.* 2012; Jackson *et al.* 2014, 2018). This would imply that Brca1 deletion data in mice models are translatable to the loss of BRCA1 in humans. The detrimental impact of skeletal muscle-specific Brca1 deletion in the present study may therefore be relevant to the maintenance of skeletal muscle quality in humans and, by extension, to the risk of developing disease, particularly those related to muscle contractile and metabolic function. Additionally, disease development and progression is a multifactorial process, such that loss of BRCA1 function in muscle may have further indirect consequences on human health that were not investigated in the current murine study.

The noted similarities between Brca1KO^{smi} mice and models of accelerated ageing are also of interest because skeletal muscle function is necessary for the preservation of functional independence and quality of life during the natural process of age-related decline. This strengthens the need to better understand the effects of *BRCA1* mutations in skeletal muscle across the lifespan and how such mutations interact with and progress age-related muscle decline and disease. Advancements in our understanding of *Brca1* functional mutations in mouse skeletal muscle can provide mechanistic insights into the role of Brca1 in skeletal muscle, and thereby direct efforts aiming to better understand the role of BRCA1 in human skeletal muscle and health.

References

Alexeyev M, Shokolenko I, Wilson G & LeDoux S (2013). The maintenance of mitochondrial DNA integrity – critical analysis and update. *Cold Spring Harb Perspect Biol* **5**, a012641–a012641.

Anon (2018). Tissue Expression of BRCA1 – Summary – The Human Protein Atlas. Available at: https://www.proteinatlas.org/ENSG00000012048-BRCA1/tissue [Accessed 9 October 2018].

Arun B, Akar U, Gutierrez-Barrera AM, Hortobagyi GN & Ozpolat B (2015). The PARP inhibitor AZD2281 (Olaparib) induces autophagy/mitophagy in BRCA1 and BRCA2 mutant breast cancer cells. *Int J Oncol* **47**, 262–268.

Bae I, Fan S, Meng Q, Rih JK, Kim HJ, Kang HJ, Xu J, Goldberg ID, Jaiswal AK & Rosen EM (2004). BRCA1 induces antioxidant gene expression and resistance to oxidative stress. *Cancer Res* **64**, 7893–7909.

Barton ER, Lynch G, Khurana TS, Grange RW, Raymackers J-M, Dorchies O & Carlson G (2008). Measuring Isometric Force of Isolated Mouse Muscles In Vitro. Available at: http://www.treat-nmd.eu/downloads/file/sops/dmd/MDX/DMD_M.1.2.002.pdf [Accessed 13 December 2017].

Bell D et al. (2011). Integrated genomic analyses of ovarian carcinoma. *Nature* **474**, 609–615.

Clark SL, Rodriguez AM, Snyder RR, Hankins GD V & Boehning D (2012). Structure-function of the tumor suppressor BRCA1. *Comput Struct Biotechnol J* **1**, e201204005.

Coene ED, Hollinshead MS, Waeytens AAT, Schelfhout VRJ, Eechaute WP, Shaw MK, Van Oostveldt PM V & Vaux DJ (2005). Phosphorylated BRCA1 is predominantly located in the nucleus and mitochondria. *Mol Biol Cell* **16**, 997–1010.

Cousineau I & Belmaaza A (2007). Cell cycle BRCA1 haploinsufficiency, but not heterozygosity for a BRCA1-truncating mutation, deregulates homologous recombination. *Cell Cycle* **6**, 962–971.

Deng C-X (2006). BRCA1: cell cycle checkpoint, genetic instability, DNA damage response and cancer evolution. *Nucleic Acids Res* **34**, 1416–1426.

Diaz F, Thomas CK, Garcia S, Hernandez D & Moraes CT (2005). Mice lacking COX10 in skeletal muscle recapitulate the phenotype of progressive mitochondrial myopathies associated with cytochrome c oxidase deficiency. *Hum Mol Genet* **14**, 2737–2748.

Dulic A, Bates PA, Zhang X, Martin SR, Freemont PS, Lindahl T & Barnes DE (2001). BRCT domain interactions in the heterodimeric DNA repair protein XRCC1-DNA ligase III. *Biochemistry* **40**, 5906–5913.

Esposito LA, Melov S, Panov A, Cottrell BA & Wallace DC (1999). Mitochondrial disease in mouse results in increased oxidative stress. *Proc Natl Acad Sci U S A* **96**, 4820–4825.

Freemont PS (2000). Ubiquitination: RING for destruction? *Curr Biol* **10**, R84–R87.

Godet I & Gilkes DM (2017). BRCA1 and BRCA2 mutations and treatment strategies for breast cancer. *Integr Cancer Sci*, https://doi.org/10.15761/ICST.1000228.

Gorrini C et al. (2013). BRCA1 interacts with Nrf2 to regulate antioxidant signaling and cell survival. *J Exp Med* **210**, 1529–1544.

Gouspillou G, Godin R, Piquereau J, Picard M, Mofarrahi M, Mathew J, Purves-Smith FM, Sgarioto N, Hepple RT, Burelle Y & Hussain SNA (2018). Protective role of Parkin in skeletal muscle contractile and mitochondrial function. *J Physiol* **596**, 2565–2579.

Hennessy BTJ, Timms KM, Carey MS, Gutin A, Meyer LA, Flake DD, Abkevich V, Potter J, Pruss D, Glenn P, Li Y, Li J, Gonzalez-Angulo AM, McCune KS, Markman M, Broaddus RR, Lanchbury JS, Lu KH & Mills GB (2010). Somatic mutations in *BRCA1* and *BRCA2* could expand the number of patients that benefit from poly (ADP ribose) polymerase inhibitors in ovarian cancer. *J Clin Oncol* **28**, 3570–3576.

Hepple RT, Krüger M, Neufer PD, Lark DS, Reese LR, Ryan TE, Torres MJ, Smith CD & Lin C-T (2015). Protein kinase A governs oxidative phosphorylation kinetics and oxidant emitting potential at complex I. *Front Physiol* **6**, 332.

Ishihara N, Fujita Y, Oka T & Mihara K (2006). Regulation of mitochondrial morphology through proteolytic cleavage of OPA1. *EMBO J* **25**, 2966–2977.

Iyer SR, Valencia AP, Hernández-Ochoa EO & Lovering RM (2016). In vivo assessment of muscle contractility in animal studies. *Methods Mol Biol* **1460**, 293–307.

Jackson KC, Gidlund E-K, Norrbom J, Valencia AP, Thomson DM, Schuh RA, Neufer PD & Spangenburg EE (2014). BRCA1 is a novel regulator of metabolic function in skeletal muscle. *J Lipid Res* **55**, 668–680.

Jackson KC, Tarpey MD, Valencia AP, Iñigo MR, Pratt SJ, Patteson DJ, McClung JM, Lovering RM, Thomson DM & Spangenburg EE (2018). Induced Cre-mediated knockdown of Brca1 in skeletal muscle reduces mitochondrial respiration and prevents glucose intolerance in adult mice on a high-fat diet. *FASEB J* **32**, 3070–3084.

Kashatus JA, Nascimento A, Myers LJ, Sher A, Byrne FL, Hoehn KL, Counter CM & Kashatus DF (2015). Erk2 phosphorylation of Drp1 promotes mitochondrial fission and MAPK-driven tumor growth. *Mol Cell* **57**, 537–551.

Kim SS, Cao L, Li C, Xu X, Huber LJ, Chodosh LA & Deng C-X (2004). Uterus hyperplasia and increased carcinogen-induced tumorigenesis in mice carrying a targeted mutation of the Chk2 phosphorylation site in Brca1. *Mol Cell Biol* **24**, 9498–9507.

Konishi H et al. (2011). Mutation of a single allele of the cancer susceptibility gene BRCA1 leads to genomic instability in human breast epithelial cells. *Proc Natl Acad Sci U S A* **108**, 17773–17778.

Kujoth GC, Hiona A, Pugh TD, Someya S, Panzer K, Wohlgemuth SE, Hofer T, Seo AY, Sullivan R, Jobling WA, Morrow JD, Van Remmen H, Sedivy JM, Yamasoba T, Tanokura M, Weindruch R, Leeuwenburgh C & Prolla TA (2005). Mitochondrial DNA mutations, oxidative stress, and apoptosis in mammalian aging. *Science* **309**, 481–484.

Lee W-K, Spielmann M, Bork U & Thévenod F (2005). Cd^{2+}-induced swelling-contraction dynamics in isolated kidney cortex mitochondria: role of Ca^{2+} uniporter, K^+ cycling, and protonmotive force. *Am J Physiol Cell Physiol* **289**, C656–C664.

Liu X, Weaver D, Shirihai O & Hajnóczky G (2009). Mitochondrial 'kiss-and-run': interplay between mitochondrial motility and fusion-fission dynamics. *EMBO J* **28**, 3074–3089.

Liu Y & West SC (2002). Distinct functions of BRCA1 and BRCA2 in double-strand break repair. *Breast Cancer Res* **4**, 9–13.

Lovren F, Pan Y, Quan A, Singh KK, Khan R, Gupta N, Brezden-Masley C, Teoh H, Wheatcroft MD, Al-Omran M & Verma S (2014). BRCA1 shields vascular smooth muscle cells from oxidative stress. *J Thorac Cardiovasc Surg* **147**, 1946–1955.e1.

Ma Q (2013). Role of nrf2 in oxidative stress and toxicity. *Annu Rev Pharmacol Toxicol* **53**, 401–426.

Magnard C, Bachelier R, Vincent A, Jaquinod M, Kieffer S, Lenoir GM & Venezia ND (2002). BRCA1 interacts with acetyl-CoA carboxylase through its tandem of BRCT domains. *Oncogene* **21**, 6729–6739.

Maniccia AW, Lewis C, Begum N, Xu J, Cui J, Chipitsyna G, Aysola K, Reddy V, Bhat G, Fujimura Y, Henderson B, Reddy ESP & Rao VN (2009). Mitochondrial localization, ELK-1 transcriptional regulation and growth inhibitory functions of BRCA1, BRCA1a, and BRCA1b proteins. *J Cell Physiol* **219**, 634–641.

Manke IA, Lowery DM, Nguyen A & Yaffe MB (2003). BRCT repeats as phosphopeptide-binding modules involved in protein targeting. *Science* **302**, 636–639.

Mehrgou A & Akouchekian M (2016). The importance of BRCA1 and BRCA2 genes mutations in breast cancer development. *Med J Islam Repub Iran* **30**, 369.

Metter EJ, Talbot LA, Schrager M & Conwit R (2002). Skeletal muscle strength as a predictor of all-cause mortality in healthy men. *Journals Gerontol Ser A Biol Sci Med Sci* **57**, B359–B365.

Miki Y, Swensen J, Shattuck-Eidens D, Futreal PA, Harshman K, Tavtigian S, Liu Q, Cochran C, Bennett LM & Ding W (1994). A strong candidate for the breast and ovarian cancer susceptibility gene BRCA1. *Science* **266**, 66–71.

Moreau K, Dizin E, Ray H, Luquain C, Lefai E, Foufelle F, Billaud M, Lenoir GM & Venezia ND (2006). BRCA1 affects lipid synthesis through its interaction with acetyl-CoA carboxylase. *J Biol Chem* **281**, 3172–3181.

Morrow RM, Picard M, Derbeneva O, Leipzig J, McManus MJ, Gouspillou G, Barbat-Artigas S, Dos Santos C, Hepple RT, Murdock DG & Wallace DC (2017). Mitochondrial energy deficiency leads to hyperproliferation of skeletal muscle mitochondria and enhanced insulin sensitivity. *Proc Natl Acad Sci U S A* **114**, 2705–2710.

Neuspiel M, Zunino R, Gangaraju S, Rippstein P & McBride H (2005). Activated mitofusin 2 signals mitochondrial fusion, interferes with Bax activation, and reduces susceptibility to radical induced depolarization. *J Biol Chem* **280**, 25060–25070.

O'Rourke AR, Lindsay A, Tarpey MD, Yuen S, McCourt P, Nelson DM, Perrin BJ, Thomas DD, Spangenburg EE, Lowe DA & Ervasti JM (2018). Impaired muscle relaxation and mitochondrial fission associated with genetic ablation of cytoplasmic actin isoforms. *FEBS J* **285**, 481–500.

Ortega FJ, Moreno-Navarrete JM, Mayas D, García-Santos E, Gómez-Serrano M, Rodriguez-Hermosa JI, Ruiz B, Ricart W, Tinahones FJ, Frühbeck G, Peral B & Fernández-Real JM (2012). Breast cancer 1 (BrCa1) may be behind decreased lipogenesis in adipose tissue from obese subjects. *PLoS ONE* **7**, e33233.

Otis JS, Roy RR, Edgerton VR & Talmadge RJ (2004). Adaptations in metabolic capacity of rat soleus after paralysis. *J Appl Physiol* **96**, 584–596.

Palmer CS, Elgass KD, Parton RG, Osellame LD, Stojanovski D & Ryan MT (2013). Adaptor proteins MiD49 and MiD51 can act independently of Mff and Fis1 in Drp1 recruitment and are specific for mitochondrial fission. *J Biol Chem* **288**, 27584–27593.

Privat M, Radosevic-Robin N, Aubel C, Cayre A, Penault-Llorca F, Marceau G, Sapin V, Bignon Y-J & Morvan D (2014). BRCA1 induces major energetic metabolism reprogramming in breast cancer cells. *PLoS ONE* **9**, e102438.

Roy R, Chun J & Powell SN (2012). BRCA1 and BRCA2: different roles in a common pathway of genome protection. *Nat Rev Cancer* **12**, 68–78.

Ruffner H, Joazeiro CA, Hemmati D, Hunter T & Verma IM (2001). Cancer-predisposing mutations within the RING domain of BRCA1: loss of ubiquitin protein ligase activity and protection from radiation hypersensitivity. *Proc Natl Acad Sci U S A* **98**, 5134–5139.

Ryan TE, Schmidt CA, Green TD, Spangenburg EE, Neufer PD & McClung JM (2016). Targeted expression of catalase to mitochondria protects against ischemic myopathy in high-fat diet-fed mice. *Diabetes* **65**, 2553–2568.

Saha T, Rih JK & Rosen EM (2009). BRCA1 down-regulates cellular levels of reactive oxygen species. *FEBS Lett* **583**, 1535–1543.

Saha T, Rih JK, Roy R, Ballal R & Rosen EM (2010). Transcriptional regulation of the base excision repair pathway by BRCA1. *J Biol Chem* **285**, 19092–19105.

Salem AF, Howell A, Sartini M, Sotgia F & Lisanti MP (2012). Downregulation of stromal BRCA1 drives breast cancer tumor growth via upregulation of HIF-1α, autophagy and ketone body production. *Cell Cycle* **11**, 4167–4173.

Satagopan JM, Offit K, Foulkes W, Robson ME, Wacholder S, Eng CM, Karp SE & Begg CB (2001). The lifetime risks of breast cancer in Ashkenazi Jewish carriers of BRCA1 and BRCA2 mutations. *Cancer Epidemiol Biomarkers Prev* **10**, 467–473.

Schiaffino S & Reggiani C (2011). Fiber types in mammalian skeletal muscles. *Physiol Rev* **91**, 1447–1531.

Schmidt CA, Ryan TE, Lin C-T, Inigo MMR, Green TD, Brault JJ, Spangenburg EE & McClung JM (2017). Diminished force production and mitochondrial respiratory deficits are strain-dependent myopathies of subacute limb ischemia. *J Vasc Surg* **65**, 1504–1514.e11.

Shokolenko I, Venediktova N, Bochkareva A, Wilson GL & Alexeyev MF (2009). Oxidative stress induces degradation of mitochondrial DNA. *Nucleic Acids Res* **37**, 2539–2548.

Shukla PC et al. (2011). BRCA1 is an essential regulator of heart function and survival following myocardial infarction. *Nat Commun* **2**, 593.

Silver DP & Livingston DM (2012). Mechanisms of BRCA1 tumor suppression. *Cancer Discov* **2**, 679–684.

Singh KK, Shukla PC, Quan A, Al-Omran M, Lovren F, Pan Y, Brezden-Masley C, Ingram AJ, Stanford WL, Teoh H & Verma S (2013). BRCA1 is a novel target to improve endothelial dysfunction and retard atherosclerosis. *J Thorac Cardiovasc Surg* **146**, 949–960.e4.

Spangenburg EE, Le Roith D, Ward CW & Bodine SC (2008). A functional insulin-like growth factor receptor is not necessary for load-induced skeletal muscle hypertrophy. *J Physiol* **586**, 283–291.

Suberbielle E, Djukic B, Evans M, Kim DH, Taneja P, Wang X, Finucane M, Knox J, Ho K, Devidze N, Masliah E & Mucke L (2015). DNA repair factor BRCA1 depletion occurs in Alzheimer brains and impairs cognitive function in mice. *Nat Commun* **6**, 8897.

Szabo CI, Wagner LA, Francisco L V, Roach JC, Argonza R, King MC & Ostrander EA (1996). Human, canine and murine BRCA1 genes: sequence comparison among species. *Hum Mol Genet* **5**, 1289–1298.

Taguchi N, Ishihara N, Jofuku A, Oka T & Mihara K (2007). Mitotic phosphorylation of dynamin-related GTPase Drp1 participates in mitochondrial fission. *J Biol Chem* **282**, 11521–11529.

Trifunovic A, Wredenberg A, Falkenberg M, Spelbrink JN, Rovio AT, Bruder CE, Bohlooly-Y M, Gidlöf S, Oldfors A, Wibom R, Törnell J, Jacobs HT & Larsson N-G (2004). Premature ageing in mice expressing defective mitochondrial DNA polymerase. *Nature* **429**, 417–423.

Venkitaraman AR (2002). Cancer susceptibility and the functions of BRCA1 and BRCA2. *Cell* **108**, 171–182.

Vermulst M, Bielas JH & Loeb LA (2008). Quantification of random mutations in the mitochondrial genome. *Methods* **46**, 263–268.

de Vries RLA, Gilkerson RW, Przedborski S & Schon EA (2012). Mitophagy in cells with mtDNA mutations. *Autophagy* **8**, 699–700.

Wang Y, Cortez D, Yazdi P, Neff N, Elledge SJ & Qin J (2000). BASC, a super complex of BRCA1-associated proteins involved in the recognition and repair of aberrant DNA structures. *Genes Dev* **14**, 927–939.

Williams RS, Bernstein N, Lee MS, Rakovszky ML, Cui D, Green R, Weinfeld M & Glover JNM (2005). Structural basis for phosphorylation-dependent signaling in the DNA-damage response. *Biochem Cell Biol* **83**, 721–727.

Yoshida K & Miki Y (2004). Role of BRCA1 and BRCA2 as regulators of DNA repair, transcription, and cell cycle in response to DNA damage. *Cancer Sci* **95**, 866–871.

Yoshikawa K, Honda K, Inamoto T, Shinohara H, Yamauchi A, Suga K, Okuyama T, Shimada T, Kodama H, Noguchi S, Gazdar AF, Yamaoka Y & Takahashi R (1999). Reduction of BRCA1 protein expression in Japanese sporadic breast carcinomas and its frequent loss in BRCA1-associated cases. *Clin Cancer Res* **5**, 1249–1261.

Yu X, Chini CCS, He M, Mer G & Chen J (2003). The BRCT domain is a phospho-protein binding domain. *Science* **302**, 639–642.

Additional information

Competing interests

The authors declare that they have no competing interests.

Author contributions

The experiments were initiated at the University of Maryland (past) with the large majority completed at East Carolina University (present). Transmission electron microscopy was conducted by RHR in the ECU EM imaging core laboratory. MDT, APV, JMM, RML and EES were responsible for the conception of the study. MDT, APV, TER, JMM, RML and EES were responsible for the study design. MDT, APV, KCJ, AJA, NPB, RHR, SJPP and EES were responsible for the acquisition of data. MDT, APV, KCJ, AJA and EES were responsible for the analysis of data. MDT, TER, JMM, RML and EES were responsible for the interpretation of data. MDT and EES were responsible for drafting the manuscript. MDT, TER, JMM, RML and EES were responsible for revising the manuscript. All authors have approved the final version of the manuscript submitted for publication, agree to be accountable for all aspects of the work, and meet the standards required for authorship. All persons meeting the standards of authorship have been included as authors.

Funding

This work was supported by the National Institutes of Health: R01AR06660 and R21AR059913 (EES); R01HL25695 (JMM); R01AR059179 and R21AR067872 (RML); and F32HL129632 (TER).